

Stellar distances from spectroscopic observations: a new technique

Benedict Burnett* and James Binney

Rudolf Peierls Centre for Theoretical Physics, Keble Road, Oxford, OX1 3NP, UK

22 April 2010

ABSTRACT

A Bayesian approach to the determination of stellar distances from photometric and spectroscopic data is presented and tested both on pseudodata, designed to mimic data for stars observed by the RAVE survey, and on the real stars from the Geneva-Copenhagen survey. It is argued that this method is optimal in the sense that it brings to bear all available information and that its results are limited only by observational errors and the underlying physics of stars. The method simultaneously returns the metallicities, ages and masses of programme stars. Remarkably, the uncertainty in the output metallicity is typically 44 per cent smaller than the uncertainty in the input metallicity.

Key words: star: distances – methods: numerical – methods: statistical – techniques: photometric – techniques: spectroscopic – astrometry

1 INTRODUCTION

Present attempts to reconcile models of the Galaxy with observations are hampered by a lack of full 6d phase space data for a large number of stars. While the majority of recent stellar surveys – for example the Geneva-Copenhagen survey (Nordström et al. 2004) and the Radial Velocity Experiment (RAVE; Steinmetz 2003) – provide sky positions, proper motions and often radial velocities, the persistent difficulty is the determination of distances, without which proper-motion measurements are of limited value. Since the fitting of models to observational constraints is arguably the method with the most potential for understanding the true nature of the Galaxy, the lack of these distance data is a key obstacle to our understanding of the Milky Way, and thus to our understanding of galaxies in general.

Several methods of distance determination are known. Perhaps most famously and successfully, the Hipparcos satellite measured trigonometric parallaxes for $\sim 10^5$ stars down to a V -band magnitude of around 12 (Perryman 1997). Trigonometric parallax is conceptually the most fundamental distance measurement technique for stars; however the Hipparcos measurements were accurate only out to a distance of around 200 pc. Within the next decade, the Gaia mission (Perryman 2005) should return parallaxes for around 10^9 stars, dramatically increasing the size of the available data set for investigation; however in the meantime trigonometric parallaxes to a vast number of otherwise well-observed stars are lacking. Furthermore, even after the Gaia mission is complete, other estimation methods will remain vital for more distant stars.

Two other trigonometric methods of distance measurement are known: so-called ‘Galactic parallax’ (Eyre & Binney 2009; Eyre 2009) and ‘geometrodynamical’ techniques (Jin & Lynden-Bell 2008). However, both these methods require strong constraints on

the orbits of target stars, so they are restricted to a small subset of all stars.

The next most reliable distance determination technique is the use of so-called ‘standard candles’ – stars with particular properties such as RR Lyrae and Cepheid variables, whose luminosities are a reasonably sharply-defined function of observables such as period and colour. While the accuracies attainable for such stars may be high, standard candles form an extremely small subset of any stellar population. Hence although they can be used to give a broad-brush picture of Galactic structure (see Gaitschy & Saio 1996), the technique cannot be applied to the majority of stars of interest.

The other major technique for distance estimation is the determination of ‘photometric distances’. This involves deducing the luminosity of a star from its colours and perhaps metallicity, allowing its distance to be inferred from its apparent magnitude. Jurić et al. (2008) have applied this technique to millions of stars measured by the Sloan Digital Sky Survey (hereafter SDSS). The technique works well for SDSS stars because they are apparently faint and therefore overwhelmingly likely to lie on the main sequence, and the luminosity of such a star is a well-defined function of colour and metallicity. However for samples at brighter apparent magnitudes it is not safe to assume that stars lie on the main sequence, and a more sophisticated technique is required.

An example of such a sample is the RAVE survey, which is in many ways complementary to the SDSS sample. It covers a nominal I -band magnitude range of $9 < I < 12$ and is expected to provide spectrophotometric data on up to a million stars by 2011 (Steinmetz et al. 2006). On account of its magnitude range, the RAVE sample contains a non-negligible number of giants. Such a heterogeneous sample therefore requires a more sophisticated approach to parameter determination than a direct colour-to-absolute magnitude mapping. Furthermore it would be much more satisfactory to obtain a methodology that can give a definitive distance esti-

* E-mail: burnett@thphys.ox.ac.uk

mation (and corresponding individual uncertainty) for specific stars rather than only for sizeable statistical samples.

Recently Breddels et al. (2010) estimated photometric distances to $\sim 25\,000$ stars in the RAVE survey. These distances were obtained by repeatedly seeking the stellar model that provides the best fit to first the data and then 5000 pseudo-data obtained by scattering the observables of the first stellar model by the observational errors. The logical justification of this procedure is unclear. In this paper we argue that the principles of Bayesian inference lead unambiguously to a different procedure that has much in common with the procedures for determining stellar ages introduced by Pont & Eyer (2004) and Jørgensen & Lindegren (2005). In fact, our procedure yields not only a distance to each star but also estimates of its mass, age and metallicity. We argue that our procedure is optimal in the sense that it exploits the available data in their entirety – including information about the survey in question. From these facts it constructs a pdf for each star in model space, so estimated distances, masses, ages and metallicities are accompanied by error estimates. The method is applicable to any survey that provides more than one non-degenerate observable for each star and is limited only by degeneracies in the underlying stellar physics and any inherent inaccuracies in the stellar models.

The paper is structured as follows: Section 2 covers the theoretical basis of the method. Section 3 explores the application of the method to a fake data set. Section 4 then looks at the results of its application to the Geneva-Copenhagen sample. Section 5 details the relationship of this paper to previous. Section 6 presents a discussion of the results and highlights the potential for future applicability.

2 THEORY

Let \mathbf{y} represent an n -tuple of a star’s observable quantities (e.g. effective temperature T_{eff} , surface gravity $\log g$, observed metallicity $[\text{M}/\text{H}]_{\text{obs}}$, colours, apparent magnitudes, sky position) and let \mathbf{x} represent its six ‘intrinsic’ variables (true initial metallicity $[\text{M}/\text{H}]$, age τ , initial mass \mathcal{M} , distance s , and true sky position (l, b) – i.e.

$$\mathbf{x} = ([\text{M}/\text{H}], \tau, \mathcal{M}, s, l, b). \quad (1)$$

We will assume that a stellar model can be used to provide a direct mapping from \mathbf{x} -space to \mathbf{y} -space. For the purpose of concision, let $G(\mathbf{w}, \boldsymbol{\sigma})$ represent the multivariate Gaussian function

$$G(\mathbf{w}, \boldsymbol{\sigma}) \equiv \prod_{i=1}^n (\sigma_i \sqrt{2\pi})^{-1} \exp(-w_i^2/2\sigma_i^2) \quad (2)$$

for an n -tuple \mathbf{w} .

In order to estimate a value and an uncertainty for each stellar parameter, the natural approach to take is probabilistic. We know a set of facts: the actual measured values of a star’s observables ($\bar{\mathbf{y}}$), the quoted errors thereon ($\boldsymbol{\sigma}_y$) and, subtly, the fact that the star is in the given sample (let this fact be denoted by S). Hence the logical distribution to consider is the pdf of a star’s parameters x_i given these three facts. If we can find this distribution, then we have all the parametric information that can logically be inferred from the known facts – most importantly, we can give an expectation value for each parameter and an estimated error on this value.

Explicitly, for each component x_i of \mathbf{x} we seek the three moments \mathcal{I}_{ik} defined by

$$\mathcal{I}_{ik} = \int x_i^k p(\mathbf{x}|\bar{\mathbf{y}}, \boldsymbol{\sigma}_y, S) d^6 \mathbf{x}, \quad (3)$$

where $k \in \{0, 1, 2\}$. (The $k = 0$ moment should properly be unity, but it is useful if the pdf is left unnormalized.) From these moments we can then infer the expectation and variance of each stellar parameter.

In order to express the pdf in terms of known distributions, it is useful to consider the full pdf

$$\begin{aligned} p(\mathbf{x}, \bar{\mathbf{y}}, \boldsymbol{\sigma}_y, S) &= p(\mathbf{x}|\bar{\mathbf{y}}, \boldsymbol{\sigma}_y, S) p(\bar{\mathbf{y}}, \boldsymbol{\sigma}_y, S) \\ &= P(S|\bar{\mathbf{y}}, \mathbf{x}, \boldsymbol{\sigma}_y) p(\bar{\mathbf{y}}|\mathbf{x}, \boldsymbol{\sigma}_y) p(\boldsymbol{\sigma}_y|\mathbf{x}) p(\mathbf{x}). \end{aligned} \quad (4)$$

Hence we can expand the pdf in a form analogous to Bayes’ theorem to give

$$p(\mathbf{x}|\bar{\mathbf{y}}, \boldsymbol{\sigma}_y, S) = \frac{P(S|\bar{\mathbf{y}}, \mathbf{x}, \boldsymbol{\sigma}_y) p(\bar{\mathbf{y}}|\mathbf{x}, \boldsymbol{\sigma}_y) p(\boldsymbol{\sigma}_y|\mathbf{x}) p(\mathbf{x})}{p(\bar{\mathbf{y}}, \boldsymbol{\sigma}_y, S)}, \quad (5)$$

which can be simplified to

$$p(\mathbf{x}|\bar{\mathbf{y}}, \boldsymbol{\sigma}_y, S) \propto P(S|\bar{\mathbf{y}}, \mathbf{x}, \boldsymbol{\sigma}_y) p(\bar{\mathbf{y}}|\mathbf{x}, \boldsymbol{\sigma}_y) p(\boldsymbol{\sigma}_y|\mathbf{x}) p(\mathbf{x}), \quad (6)$$

wherein factors independent of \mathbf{x} have been neglected as irrelevant to the problem we aim to solve, since we will require only ratios of different \mathcal{I}_{ik} ’s.

Each of the factors in equation (6) can now be analysed independently:

(i) $P(S|\bar{\mathbf{y}}, \mathbf{x}, \boldsymbol{\sigma}_y)$, which we term the *selection function*, expresses the probability of a star being in the sample given its inherent values and the measurement errors. This factor therefore reflects our selection criteria, whether they be, for instance, a magnitude cut or any cut on errors used to ‘clean’ a sample.

(ii) For many types of observation the *likelihood* $p(\bar{\mathbf{y}}|\mathbf{x}, \boldsymbol{\sigma}_y)$ can be approximated by a Gaussian $G(\bar{\mathbf{y}} - \mathbf{y}(\mathbf{x}), \boldsymbol{\sigma}_y)$. More generally it takes a functional form determined purely by the measuring instrument, in which the different components of $\bar{\mathbf{y}}$ may or may not be independent.

(iii) $p(\boldsymbol{\sigma}_y|\mathbf{x})$ is the probability of the quoted errors in \mathbf{y} given the object’s underlying characteristics \mathbf{x} .

(iv) $p(\mathbf{x})$ is our *prior*. This will describe as many stellar populations as we wish to take into account, in terms of an initial mass function (IMF) and a spatial distribution. It describes the relative abundance of stars of various types, without regard to their observability.

The uncertainties on the observed values of (l, b) are assumed to be sufficiently small for us to regard the corresponding pdfs as delta functions and drop the integrals over l and b , leaving a 4-dimensional integral in \mathbf{x} . However, when this is done, any locational factors in the prior must gain a multiplicative factor of s^2 in order to take account of the conical shape of the volume surveyed.

In this work we assume a uniform distribution for $p(\boldsymbol{\sigma}_y|\mathbf{x})$; although in reality this will not be the case (for instance, more distant stars will tend to have higher errors), the dependence of $\boldsymbol{\sigma}_y$ on \mathbf{x} will generally be sufficiently weak not to affect our results greatly. In this case, equation (6) simplifies to

$$p(\mathbf{x}|\bar{\mathbf{y}}, \boldsymbol{\sigma}_y, S) \propto P(S|\bar{\mathbf{y}}, \mathbf{x}, \boldsymbol{\sigma}_y) p(\bar{\mathbf{y}}|\mathbf{x}, \boldsymbol{\sigma}_y) p(\mathbf{x}). \quad (7)$$

This can be substituted into the simplified form of equation (3),

$$\mathcal{I}_{ik} = \int x_i^k p(\mathbf{x}|\bar{\mathbf{y}}, \boldsymbol{\sigma}_y, S) d^4 \mathbf{x}, \quad (8)$$

giving a set of three integrals that together will give us an estimated parameter value for each star ($\langle x_i \rangle = \mathcal{I}_{i1}/\mathcal{I}_{i0}$) and an uncertainty thereon ($\sigma_i = \sqrt{(\mathcal{I}_{i2}/\mathcal{I}_{i0}) - \langle x_i \rangle^2}$), taking into account all of the known information. Thus in a single pass we can infer all these values for each star’s metallicity, age, mass and distance.

2.1 Selection function

The nature of the selection function $P(S|\bar{y}, \mathbf{x}, \sigma_y)$ bears comment, as it is by no means trivial. We must distinguish carefully what is meant by the symbol \bar{y} in the formalism above: it refers to the actual observed parameters of the star, but only those we actually use in the analysis. There may be other parameters that have been observed and enter into the selection function. If this is the case, they can be expressed only as probabilities dependent on \mathbf{x} , not on \bar{y} . Therefore it becomes important to split the selection function into two parts, one dependent on \bar{y} and the other on \mathbf{x} :

$$P(S|\bar{y}, \mathbf{x}, \sigma_y) = \psi(\bar{y}, \sigma_y) \phi(\mathbf{x}). \quad (9)$$

In this product ψ will generally be the dominant factor for two main reasons:

- (i) If the sample is based on an input catalogue, it will frequently be a selection on observables that are not then reobserved – for example, the Geneva-Copenhagen survey (Nordström et al. 2004) was selected on the basis of the Strömgren photometry of Olsen (1983, 1993, 1994a,b), which is simply transcribed to the Geneva-Copenhagen catalogue.
- (ii) The fundamental limitations on stellar photometry also tend to make ψ dominant: saturation leads to a bright-end cut being imposed on the survey; at the faint end a cutoff is imposed to eliminate objects too faint for the detector’s source extraction algorithm to distinguish true signals from noise. Both cuts are generally imposed on the basis of the observed magnitude and therefore are functions of the observed properties of a star *after scattering by observational errors*. That is, they are functions of \bar{y} rather than \mathbf{x} .

However, there can be contributions of the nature of $\phi(\mathbf{x})$, and these are of much greater importance to our analysis. For example, we will later be interested in comparison of the results provided by our method on a real stellar sample with those of the Hipparcos satellite. In such cases, it is common (e.g. Breddels et al. 2010) to consider only those stars for which Hipparcos provides reasonably well-constrained distances, by restricting the sample to stars with fractional parallax errors below a certain threshold. It is important to recognize that this induces a bias in the sample: by considering only those stars with, say, $\sigma_\varpi/\overline{\varpi} < 20\%$ (where $\overline{\varpi}$ represents the observed parallax and σ_ϖ the error thereon), one will preferentially cut away stars with low parallaxes and hence large distances, leaving a sample biased towards small distances.

This effect can, however, be at least mitigated by a consideration of the rôle of $\phi(\mathbf{x})$. For any value of \mathbf{x} , and hence a ‘true’ model distance s , it is possible to define a pdf for a star’s observed parallax $\overline{\varpi}$ from a knowledge of σ_ϖ , assuming Gaussian errors: indeed

$$p(\overline{\varpi}|s) = G(\overline{\varpi} - 1/s, \sigma_\varpi). \quad (10)$$

Therefore one can incorporate this bias into one’s analysis in the form

$$\phi(\mathbf{x}) \propto \int_{5\sigma_\varpi}^{\infty} G(\overline{\varpi} - 1/s, \sigma_\varpi) d\overline{\varpi}, \quad (11)$$

providing an element of balance in the analysis that maximum-likelihood techniques neglect.

If one can, as will generally be the case at least approximately, decompose the selection function into the form $\psi(\bar{y}, \sigma_y) \phi(\mathbf{x})$, then since we are interested only in terms dependent on \mathbf{x} , we can ignore any occurrence of $\psi(\bar{y}, \sigma_y)$. Hence our final formula for the moments of a star’s pdf collapses to

$$\mathcal{I}_{ik} = \int x_i^k \phi(\mathbf{x}) p(\bar{y}|\mathbf{x}, \sigma_y) p(\mathbf{x}) d^4\mathbf{x}, \quad (12)$$

which can be readily calculated.

2.2 Implementation

Since for many surveys the errors on apparent magnitude are very small, the integration of equation (12) need only cover a small range in distance for each set of $([M/H], \tau, \mathcal{M})$ values. Consequently, after experimenting with both fixed-grid and Markov Chain Monte Carlo techniques, it was decided that the best compromise between speed and reliability was provided by a simple fixed-grid Newton-Cotes rectangle integration method, where one defines a grid of points in metallicity, the logarithm of age, and mass. For each point in this three-dimensional space one then integrates over a range in distance corresponding to an apparent magnitude spread of say ten times the magnitude error either side of the observed value – any distances beyond this range will give a negligible contribution to the integral due to the Gaussian factor in the likelihood term $p(\bar{y}|\mathbf{x}, \sigma_y)$. For the purposes of calculating the integral it was found to be sufficient simply to multiply the integrand’s value at each grid point by an effective volume determined by the distance between the given grid point and its nearest neighbours.

No two numbers completely characterize a general probability distribution. Medians, means and modes can all be used to characterize the centre of the distribution. The median is the most stable measure and generally to be preferred. Unfortunately, it is in general hard to calculate. The mode, which was favoured by Jørgensen & Lindegren (2005), is susceptible to noise when the distribution is at all flat-topped. Therefore we favour the mean as a robust and readily calculated measure of the pdf. Similarly, we favour the variance as an estimate of the width of the pdf, rather than the more complex confidence intervals used by Jørgensen & Lindegren.

Another advantage of using these two numbers to characterize the distribution is that their calculation, via the integration technique outlined above, avoids the thorny issue of interpolation on the isochrones by considering only the values of observables at tabulated grid points. Interpolation using isochrones is notoriously difficult, and thus we avoid it as far as is possible.

To summarize, the method we propose runs as follows:

- (i) Define a grid of points in $([M/H], \log \tau, \mathcal{M})$ space. We found a suitable grid spacing to be given by the metallicity values given in Table 2 (although a greater range would do no harm – one should include the lowest metallicity that is available from the isochrones); a spacing in $\log \tau$ of 0.025; and the mass spacing provided automatically by the Padova isochrones, which ranges from $10^{-6} M_\odot$ to $0.255 M_\odot$.

- (ii) At each grid point, define a further set of points in distance s , covering the range

$$s \in [r(m - n\sigma_m), r(m + n\sigma_m)], \quad (13)$$

where m is the apparent magnitude used for fitting to observations, σ_m is the observational error thereon, and $r(m)$ represents the distance that produces an apparent magnitude of m given the metallicity, age and mass at the grid point in question. n is some positive number chosen by the user – we found $n = 5$ to be ample for high precision.

- (iii) Assign to each point a 4-volume corresponding to a hypercuboid with boundary planes halfway to each of the point’s nearest

neighbours (at the edges of parameter space, take the length in the limiting dimension to be that between the final two data points).

(iv) Perform the integral in equation (12) by finding the value of $\phi(\mathbf{x})p(\bar{\mathbf{y}}|\mathbf{x}, \sigma_y)p(\mathbf{x})$ at each grid point, multiplied by the grid point's associated 4-volume. We term this product of probability density and volume the 'weight' of each grid point. For each of the first four dimensions of \mathbf{x} , one can then define an array that keeps track of the sum of these weights multiplied by powers of each parameter x_i , and also keep a running total of the sum of the weights themselves, which we term \mathcal{I}_0 .

(v) Once one has run over the entire grid (or some subset thereof, since one may be able to disregard metallicities too far from the observed value), one can then calculate the moments \mathcal{I}_{ik} by dividing each running total by \mathcal{I}_0 . From the \mathcal{I}_{ik} one then has directly an expectation and uncertainty for each dimension of \mathbf{x} .

(vi) It is of course imperative to check that one has sampled \mathbf{x} -space sufficiently finely to achieve sufficient precision in the work. For these purposes one should redo the analysis of a sample of stars using a finer sampling in each dimension and check that there is minimal alteration in the outputs for the new sampling. If time is not a concern, one would ideally do this for every star, refining the grid iteratively to a point where there is minimal change in the outputs. This may require interpolation if the isochrones cannot be provided with a fine enough sampling.

2.3 Terminology

In what follows, we shall refer to the technique described above as the 'Bayesian method', in order to distinguish it from what we shall call the 'maximum-likelihood method'. The distinction here essentially concerns the nature of the prior and selection function. Maximum-likelihood techniques for fitting a model to data consist of finding the model (from some specified range) that maximizes the probability of the data in question – i.e. in our case one would seek to maximize the likelihood $p(\bar{\mathbf{y}}|\mathbf{x}, \sigma_y)$. This is mathematically equivalent to setting both the selection function and the prior in the above formalism to uniform distributions, but conceptually it has an important difference from our Bayesian approach, which seeks to find the model with the maximum probability of being correct given the data. Maximum-likelihood techniques are popular due to their simplicity – they involve no consideration of the nature of the prior and they generally do not take into account the selection function. Furthermore, from a conceptual viewpoint, the Bayesian technique is a more justified approach to the problem of model selection than maximum likelihood: since the data are given, it is logical to seek the model with the maximum probability of being correct given the data. For the case of determining stellar ages, Jørgensen & Lindegren (2005) give a nice example of the advantage of a Bayesian approach over maximum likelihood, while Pont & Eyser (2004) provide an extensive discussion of the relative merits of a Bayesian technique.

One more point bears comment with regard to maximum likelihood (and naïve Bayesian approaches) when the prior is set to be uniform in order to represent an unprejudiced starting assumption. For a uniform continuous pdf, the prior can only be defined to be uniform in a specific coordinate system: a transformation of those coordinates will in general not leave it so. Thus, for example, while a uniform prior in age may seem a reasonable starting point, it is difficult to justify such an assumption as opposed to a prior uniform in e.g. the logarithm of age. Thus the assumption of a uniform prior in some space is nonetheless an assumption, and cannot be considered safer than making an explicit choice of prior after con-

sidering all the circumstances of the particular case. In general one hopes for the likelihood function to be sufficiently strongly peaked at some value to render the exact form of the prior unimportant for the posterior distribution; however in such complex, degenerate cases as those addressed here involving stellar evolution, such hopes are not always well-founded. For this reason a prior that is based on what we do know of stars in the Galaxy is an important factor in any calculation.

3 TEST CASE

3.1 Sample

In order to test the consistency of the method, a fake data set was generated to mimic the sample observed by RAVE. For these purposes, the vector of observables was taken to be

$$\mathbf{y} = (\log T_{\text{eff}}, \log g, [\text{M}/\text{H}]_{\text{obs}}, J - K, J, I, l, b), \quad (14)$$

where I , J and K denote apparent magnitudes. (Here, and throughout this paper, logarithms are taken to base 10.) Stars were generated by a Markov Chain following the Metropolis-Hastings algorithm (Saha 2003) in \mathbf{x} -space, with observational errors added in \mathbf{y} -space at every step. Since the aim was to reproduce the joint pdf described by equation (4), at every proposed point in \mathbf{x} -space, a $\bar{\mathbf{y}}$ value was generated by Gaussian scattering by a vector of observational errors, and the probability $P(S|\bar{\mathbf{y}}, \mathbf{x}, \sigma_y)$ was calculated; the acceptance was then based on the new value of $P(S|\bar{\mathbf{y}}, \mathbf{x}, \sigma_y)p(\mathbf{x})$.

The Markov chain was generated using a Gaussian proposal density, and ensuring an acceptance rate of order 30% by tuning the spread of the proposal density during a burn-in period of 10 000 steps. The chain itself consisted of 2.5×10^6 steps, of which forty-nine out of every fifty were then discarded (in order to minimize the chance of repeated \mathbf{x} -points) to provide the output 50 000 stars. Convergence was verified by performing an identical run with the selection function switched off, and ensuring that the marginalized distributions in \mathbf{x} corresponded to those input in the prior.

The Gaussian observational errors were added using an error 8-tuple

$$\sigma_y = (0.0434, \gamma(\bar{y}_1), 1.07 \bar{y}_1 - 3.71, 0.045, 0.023, 0.04, 0, 0), \quad (15)$$

where

$$\gamma(x) = \begin{cases} 0.5 & \text{if } x < \log(8000), \\ 0.25 + 0.436(x - \log(8000)) & \text{otherwise;} \end{cases} \quad (16)$$

designed to be representative of the scale of observational errors in RAVE. Errors on logarithmic quantities are measured in dex. (Although the true errors on $\log T_{\text{eff}}$ and other derived observables may not actually be Gaussian, it was considered to be a sufficient approximation for this proof-of-concept. A different error distribution could be employed very easily.) The pseudodata were therefore generated according to a distribution function described by

$$f(\mathbf{x}, \bar{\mathbf{y}}) = p(\mathbf{x}, \bar{\mathbf{y}}, \sigma_y|S) \propto P(S|\bar{\mathbf{y}}, \mathbf{x}, \sigma_y)p(\bar{\mathbf{y}}|\mathbf{x}, \sigma_y)p(\mathbf{x}), \quad (17)$$

where the factors on the right are as follows:

For the prior we took a three-component Milky Way model of the form

$$p(\mathbf{x}) = p(\mathcal{M}) \sum_{i=1}^3 p_i([\text{M}/\text{H}]) p_i(\tau) p_i(\mathbf{r}), \quad (18)$$

Table 1. Values of disc parameters used.

Parameter	Value (pc)
R_d^{thin}	2 600
z_d^{thin}	300
R_d^{thick}	3 600
z_d^{thick}	900

where $i = 1, 2, 3$ correspond to a thin disc, thick disc and stellar halo, respectively. We assumed an identical Kroupa-type IMF for all three components and distinguish them as follows:

Thin disc ($i = 1$):

$$\begin{aligned}
 p_1([\text{M}/\text{H}]) &= G([\text{M}/\text{H}], 0.2), \\
 p_1(\tau) &\propto \exp(0.119 \tau/\text{Gyr}) \quad \text{for } \tau \leq 10 \text{ Gyr}, \\
 p_1(\mathbf{r}) &\propto \exp\left(-\frac{R}{R_d^{\text{thin}}} - \frac{|z|}{z_d^{\text{thin}}}\right);
 \end{aligned} \tag{19}$$

Thick disc ($i = 2$):

$$\begin{aligned}
 p_2([\text{M}/\text{H}]) &= G([\text{M}/\text{H}] + 0.6, 0.5), \\
 p_2(\tau) &\propto \text{uniform in range } 8 \leq \tau \leq 12 \text{ Gyr}, \\
 p_2(\mathbf{r}) &\propto \exp\left(-\frac{R}{R_d^{\text{thick}}} - \frac{|z|}{z_d^{\text{thick}}}\right);
 \end{aligned} \tag{20}$$

Halo ($i = 3$):

$$\begin{aligned}
 p_3([\text{M}/\text{H}]) &= G([\text{M}/\text{H}] + 1.6, 0.5), \\
 p_3(\tau) &\propto \text{uniform in range } 10 \leq \tau \leq 13.7 \text{ Gyr}, \\
 p_3(\mathbf{r}) &\propto r^{-3.39};
 \end{aligned} \tag{21}$$

where R signifies Galactocentric cylindrical radius, z cylindrical height and r spherical radius. The parameter values were taken as in Table 1; the values are taken from the analysis of SDSS data in Jurić et al. (2008). The metallicity and age distributions for the thin disc come from Haywood (2001) and Aumer & Binney (2009), while the radial density of the halo comes from the ‘inner halo’ detected in Carollo et al. (2009). The metallicity and age distributions of the thick disc and halo are influenced by Reddy (2009) and Carollo et al. (2009).

The normalizations were then adjusted so that at the solar position, taken as $R_0 = 8.33$ kpc (Gillessen et al. 2009), $z_0 = 15$ pc, we have number density ratios $n_2/n_1 = 0.15$ (Carollo et al. 2009), $n_3/n_1 = 0.005$ (Jurić et al. 2008).

The IMF chosen follows the form originally proposed by Kroupa et al. (1993), with a minor modification following Aumer & Binney (2009), being

$$p(\mathcal{M}) \propto \begin{cases} \mathcal{M}^{-1.3} & \text{if } \mathcal{M} < 0.5 M_\odot, \\ 0.536 \mathcal{M}^{-2.2} & \text{if } 0.5 M_\odot \leq \mathcal{M} < 1 M_\odot, \\ 0.536 \mathcal{M}^{-2.519} & \text{otherwise.} \end{cases} \tag{22}$$

We determined \mathbf{y} as a function of \mathbf{x} from the isochrones of the Padova group (Bertelli et al. 2008), which provide tabulated values for the observables of stars with metallicities ranging upwards from around $[\text{M}/\text{H}] \approx -0.92$, ages in the range $\tau \in [0.01, 19]$ Gyr and masses in the range $\mathcal{M} \in [0.15, 20] M_\odot$. We used isochrones for 16 metallicities as shown in Table 2, selecting the helium mass fraction Y as a function of metal mass fraction Z according to the relation used in Aumer & Binney (2009), i.e. $Y \approx 0.225 + 2.1Z$ and

Table 2. Metallicities of isochrones used, taking $(Z_\odot, Y_\odot) = (0.017, 0.260)$.

Z	Y	[M/H]
0.0022	0.230	-0.914
0.003	0.231	-0.778
0.004	0.233	-0.652
0.006	0.238	-0.472
0.008	0.242	-0.343
0.010	0.246	-0.243
0.012	0.250	-0.160
0.014	0.254	-0.090
0.017	0.260	0.000
0.020	0.267	0.077
0.026	0.280	0.202
0.036	0.301	0.363
0.040	0.309	0.417
0.045	0.320	0.479
0.050	0.330	0.535
0.070	0.372	0.727

assuming solar values of $(Y_\odot, Z_\odot) = (0.260, 0.017)$. The metallicity values were selected by eye to ensure that there was not a great change in the stellar observables between adjacent isochrone sets.

The selection function $P(S|\bar{\mathbf{y}}, \mathbf{x}, \boldsymbol{\sigma}_y)$ was chosen to describe RAVE’s selection criteria. RAVE observes stars with nominal DENIS I -band magnitudes in the range $9 < I_{\text{DENIS}} < 12$; however Zwitter et al. (2008) explain that the upper limit actually extends up to one magnitude fainter, and that there is evidence of saturation around $I_{\text{DENIS}} < 10$. For these reasons it was decided to take the full range of I -band magnitudes observable by RAVE to be $4 < \bar{I} < 13$, and to disallow stars falling outside this range. Although the brighter limit may seem overly permissive, its actual value has little importance due to the other major factor in $P(S|\bar{\mathbf{y}}, \mathbf{x}, \boldsymbol{\sigma}_y)$: a completeness term. Although RAVE is theoretically capable of observing all stars within its magnitude limits, it is not a complete survey and thus stars at certain magnitudes have a higher probability of being included in the catalogue than others. For the purposes of this test, it was decided to use an approximation of fig. 4 of Steinmetz et al. (2006), of the form

$$P(S|\bar{\mathbf{y}}, \mathbf{x}, \boldsymbol{\sigma}_y) \propto 2.9 G(\bar{I} - 9.8, 0.76) + G(\bar{I} - 11.7, 0.51). \tag{23}$$

While this neglects variations in completeness with sky position, it seems a reasonable approximation for our pseudodata. The functional form results in stars with particularly bright apparent magnitudes being given very low weight irrespective of our chosen value for RAVE’s low- \bar{I} cutoff.

The other factor included was a cutoff at Galactic latitudes of $|b| \leq 25^\circ$, since RAVE avoids regions close to the Galactic plane. This has the obvious effect of biasing the sample slightly towards thick-disc and halo stars. (It also prevents any density divergence near the Galactic centre due to the halo density profile.)

3.2 Results

50 000 stars were generated according to the above model. Interpolation in the isochrones was necessary for these purposes; since the chosen sampling of the isochrones was reasonably dense it was decided to use linear interpolation rather than a more complex and arbitrary method. The density of the sampling points should en-

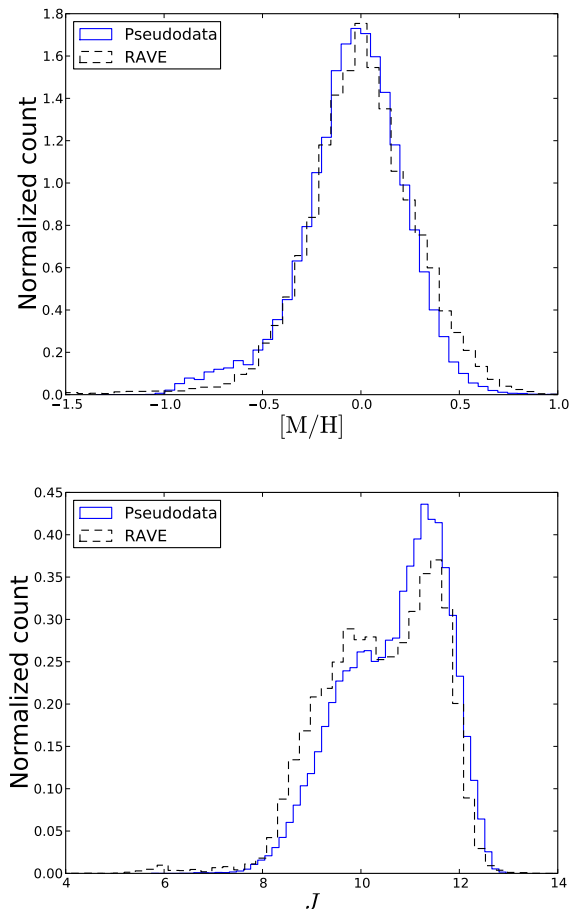


Figure 1. Distribution in metallicity (upper plot) and J -magnitude (lower plot) for the pseudodata (full lines) and stars in the RAVE catalogue (dashed lines).

sure that any errors introduced by this interpolation technique are minimal, and certainly sufficiently small for the present testing purpose. The resultant distributions in metallicity and in J magnitude are displayed in Fig. 1, along with that of the second data release of the RAVE survey (Zwitter et al. 2008), showing that the sample is a reasonable mimic. This sample was then analysed using the technique expounded in Section 2. The y -space fitting (the likelihood term $p(\bar{\mathbf{y}}|\mathbf{x}, \sigma_y)$) was performed in the first five components of \mathbf{y} . It was decided against using the I -band for analysis due to the saturation concerns described above, and the consequent fear that the I -magnitudes of model stars will not correspond to the I_{DENIS} system. The same reliability fear militates against considering $I(\mathbf{x})$ in the factor $\phi(\mathbf{x})$. The factor $p(\mathbf{x})$ was initially given the same form for the analysis as for the sample generation, while the factor $\phi(\mathbf{x})$ was taken to be flat, since the selection function was entirely a function of $\bar{\mathbf{y}}$.

In order to perform the integration of equation (12), we followed the prescription of Section 2. After trying various subdivisions of \mathbf{x} -space, it was determined that the optimal subdivision, balancing speed against accuracy, was obtained by taking the grid-points of the integration at the metallicity values found in Table 2, increments of 0.025 in $\log(\tau/\text{Gyr})$, and the non-uniform mass spacing provided by the isochrones. Integration in these three dimensions was performed over the entire isochrone range. The dis-

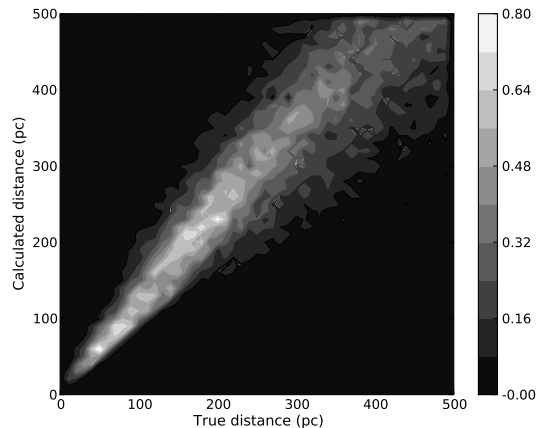


Figure 2. Density plot of the relationship of calculated to true distance for stars out to 500 pc. Contours measure density in points pc^{-2} .

tance integration was performed using $n = 5$ in equation (13) for the apparent J -magnitude, with 5 distance points used for each point in $([M/H], \log \tau, \mathcal{M})$. Using more points than this was found to give negligible improvement in results, since the actual spread for each $([M/H], \log \tau, \mathcal{M})$ value is extremely small due to the tiny values of σ_J in the 2MASS survey (~ 0.023 mag, Skrutskie et al. 2006), and correspondingly in the RAVE sample.

The results of the analysis are displayed in Figs. 2 and 3. Fig. 3 displays a histogram of the difference between the calculated value of each star’s distance and its true value, divided by the distance uncertainty σ_s returned by the method. Although it can be clearly seen that the distribution is skewed (indeed we have no a priori reason to expect it not to be), it is *not* biased: the distribution displayed has a mean value of 0.009 and a dispersion of 0.93, giving a reasonable sign that individual error estimates are trustworthy. For comparison, a fit using a simple maximum-likelihood method (i.e. dropping the factor $p(\mathbf{x})$ from the analysis) is displayed in Fig. 4. The mean of the distribution shown in the top panel of Fig. 4 is 0.15, with a dispersion of 0.68; this bias confirms the criticism of flat priors in Section 2.3. It is noteworthy that this bias persists despite the fact that the output uncertainties are significantly larger in the maximum-likelihood case, as demonstrated by the bottom panel of Fig. 4 (indeed, the small dispersion of the top panel of this figure implies that these uncertainties are systematically over-estimated). Furthermore, the positive wing displayed in the middle panel of Figs. 3 and 4 is notably more pronounced in the maximum-likelihood case. Hence it can be seen that the method outstrips standard photometric distance determination techniques.

In the case of an analysis of real stellar survey data, the prior will not be known to perfect precision. Consequently, we have also performed the analysis with two different incorrect priors, each consisting of a single stellar population:

Approximate prior 1:

$$\begin{aligned}
 p([M/H]) &= G([M/H] + 0.12, 0.2), \\
 p(\tau) &\propto \exp(0.119 \tau/\text{Gyr}) \quad \text{for } \tau \leq 10 \text{ Gyr}, \\
 p(\mathcal{M}) &\propto \mathcal{M}^{-2.35}, \\
 p(\mathbf{r}) &\propto \exp\left(-\frac{R}{2000 \text{ pc}} - \frac{|z|}{400 \text{ pc}}\right).
 \end{aligned} \tag{24}$$

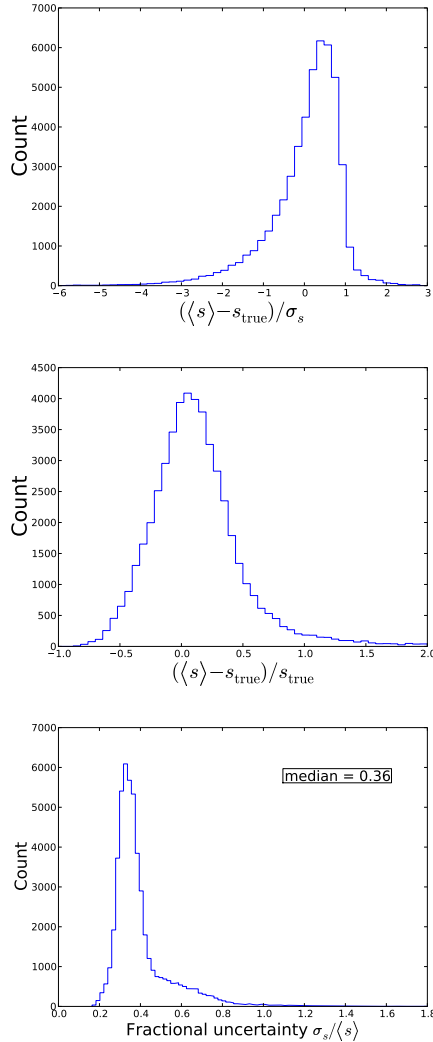


Figure 3. Results of analysis using the Bayesian method. Top panel: distribution of normalized residuals. While the distribution is skewed, it is almost entirely unbiased. Middle panel: distribution of residuals as a fraction of true distance. Bottom panel: distribution of fractional uncertainties.

Approximate prior 2:

$$\begin{aligned}
 p(\text{[M/H]}) &= G(\text{[M/H]}, 0.3), \\
 p(\tau) &\propto \exp(0.13 \tau / \text{Gyr}) \quad \text{for } \tau \leq 10 \text{ Gyr}, \\
 p(\mathcal{M}) &\propto \mathcal{M}^{-2.35}, \\
 p(\mathbf{r}) &\propto \exp\left(-\frac{R}{2000 \text{ pc}} - \frac{|z|}{400 \text{ pc}}\right).
 \end{aligned} \tag{25}$$

Fig. 5 shows the results of the analysis of our pseudodata using each of these priors. The results are remarkably good, aligning extremely closely with those using the correct prior. This is very encouraging, as it implies that the use of an approximate prior in the analysis of a real sample will give very reliable results. Most importantly, the results in Fig. 5 are incontrovertibly better than those of Fig. 4, signalling that the use of an approximate prior in any photometric distance determination *must* be preferred to the use of a flat prior – maximum-likelihood techniques are sub-optimal in such a complex situation.

Fig. 6 displays the uncertainty histogram produced from anal-

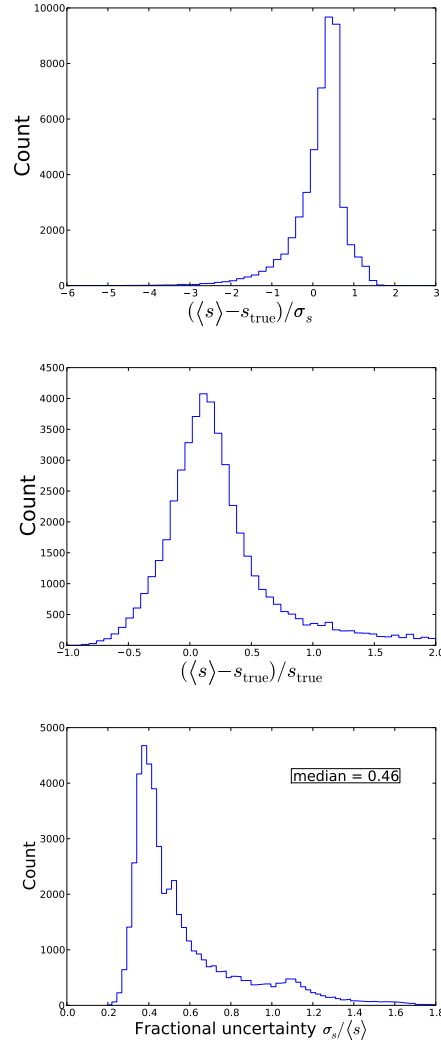


Figure 4. As Fig. 3, but for a maximum-likelihood method.

ysis of a sample generated in exactly the same way as before, except with the observational error on $\log g$ halved to $\sigma_{\log g}(\bar{y}_1) = 0.5 \gamma(\bar{y}_1)$ dex. When analysed with corresponding uncertainty included, there is a dramatic improvement in the accuracy obtained (the curve labelled ‘half error’). This is not surprising, since surface gravity is the key discriminant in differentiating between giants and dwarfs, and since the difference in brightness between the two species is so vast, any improvement in our ability to discriminate between them will rapidly decrease the uncertainty of our distance estimate. Quantitatively, halving the error in $\log g$ reduces the uncertainty in the distance by a factor of order 23%. Hence it is of the utmost importance to beat down observational errors in measurements of $\log g$ whenever photometric distances are to be obtained.

The negative wing of the distribution shown in the top panel of Fig. 3 is largely composed of stars that are best modelled as old stars ($\tau \geq 6$ Gyr) of around one solar mass. The underestimation of the uncertainties on such stars stems from the high weight that the prior assigns to such stars; if the data can be matched by such a star, the probability of this match is high and the uncertainty in

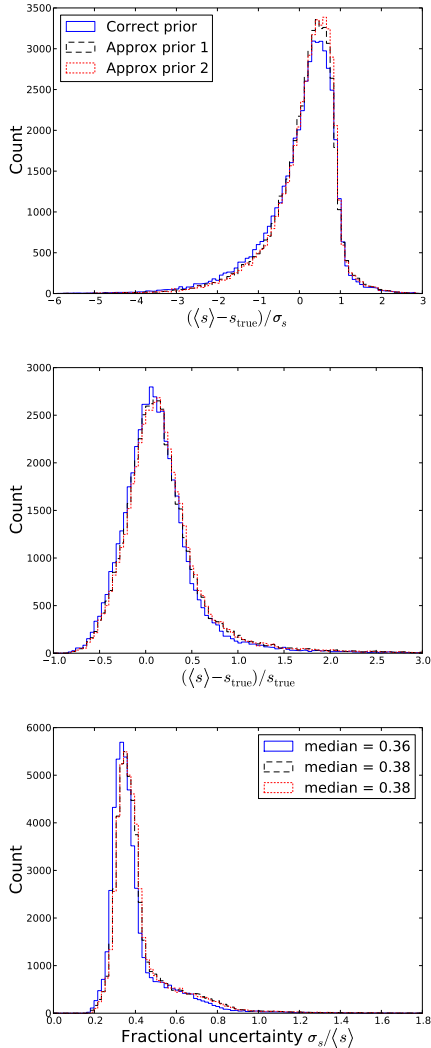


Figure 5. As Fig. 3, but using two flawed priors as described in the text. Blue line, full: correct prior; Black line, dashed: approximate prior 1; Red line, dotted: approximate prior 2.

the distance is dominated by the small error in the star’s apparent magnitude.

3.3 Metallicities, ages and masses

Figs. 8–10 show the performance of our method in the recovery of metallicities, ages and masses. Fig. 8 shows that there is minimal bias in all three measurements, and that the estimated uncertainties are reliable. Furthermore, Fig. 10 shows that with estimates of the assumed precision (0.043 dex in T_{eff} , ~ 0.5 dex in $\log g$, ~ 0.3 dex in $[M/H]$, 0.045 mag in $J - K$ and 0.023 mag in J) stellar parameters can be determined with good precision. Remarkably, the output uncertainties in $[M/H]$ are strongly peaked at ~ 0.18 dex, significantly smaller than the ‘observational’ errors (~ 0.32 dex, see Fig. 7). This reduction in uncertainty is made possible by simultaneously using all available information, which includes the physics of stellar evolution and the morphology of the Galaxy; it is not in any sense a ‘creation of information’. The errors given in the RAVE catalogue are conservatively large to allow for imperfections in the calibration data sets (Zwitter et al. 2008). They are,

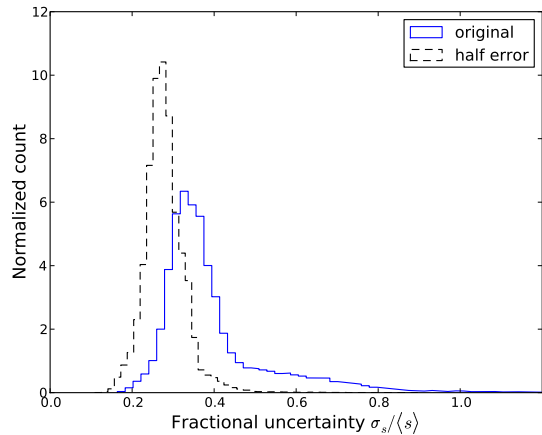


Figure 6. Normalized distribution of quoted fractional uncertainties from analysis of both the original pseudodata, with full $\sigma_{\log g}$ (‘original’) and data with half of this gravity error (‘half error’).

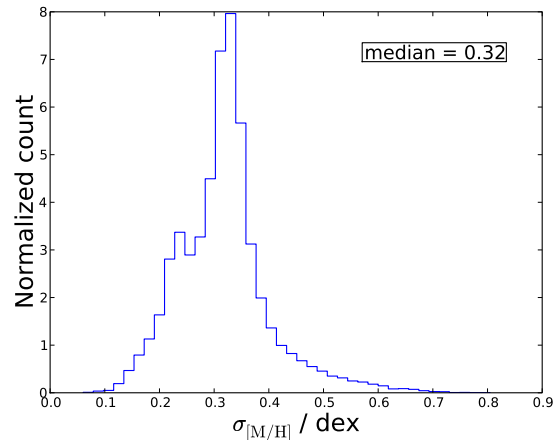


Figure 7. Histogram of the quoted ‘observational’ metallicity errors in our pseudodata.

moreover, based on the analysis of individual stellar spectra, without regard to the known properties of the population from which the individual star is drawn. It is to be expected that the injection of prior information about the Galaxy’s stellar populations and the information carried by the photometry diminishes the uncertainty on the metallicity of each star.

Also included in Fig. 8 are the results obtained with the poor prior. It can be seen that only the metallicity results are particularly altered, which is extremely promising: the bad input prior (a Gaussian centred on the wrong value) could have been dismissed a priori by comparison with the observed metallicity distribution of the sample, and thus metallicity space is in fact the least at risk from such effects. Consequently the biasing seen in the first panel of Fig. 8 is unrealistically pronounced.

One final note: while extinction and reddening have not been included in this work, any model of these effects could be included in the analysis simply by altering the dependence of colours and magnitude on position.

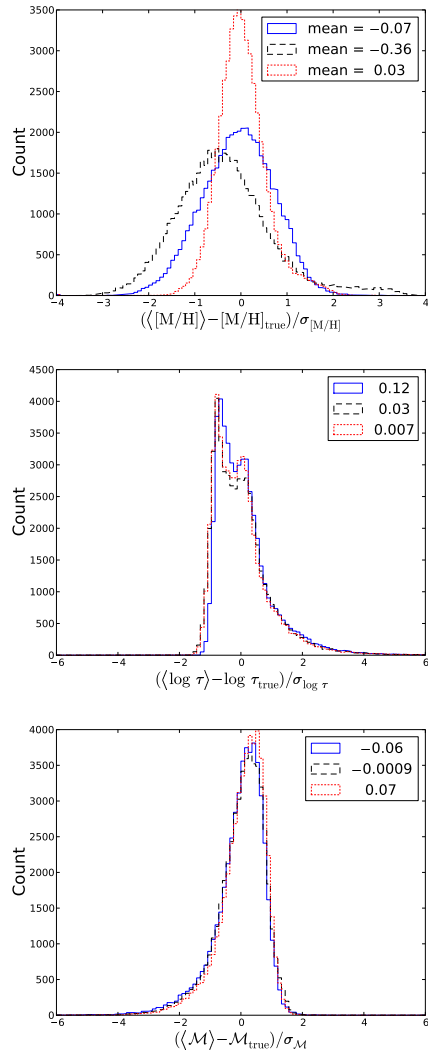


Figure 8. Distributions of residuals in $[M/H]$, $\log \tau$ and \mathcal{M} normalized by the corresponding uncertainties for the pseudodata using the correct prior and using the approximate priors. Blue line, full: correct prior; Black line, dashed: approximate prior 1; Red line, dotted: approximate prior 2. The mean is displayed for each distribution.

4 REAL-WORLD TESTING: THE GENEVA-COPENHAGEN SAMPLE

The previous section demonstrated the success of the method applied to a well-controlled sample of pseudodata. Here we inspect its performance when applied to real-world data, with all of its associated noise and limitations. To this end we have analysed the Geneva-Copenhagen survey data (Holmberg et al. 2009), selecting all stars with Hipparcos parallaxes.

Since error propagation from parallax to distance space is not trivial for stars with sizeable fractional parallax errors, it is best to perform the comparison in parallax space itself. Our method can provide an estimated value and uncertainty for each star’s parallax as easily as its distance and with equal validity, so this comparison is a simple matter. This also permits comparison with a larger sample of stars than would be permitted in distance space, since even stars with negative Hipparcos parallaxes can be used in a parallax-space comparison. Consequently the subtle biasing in-

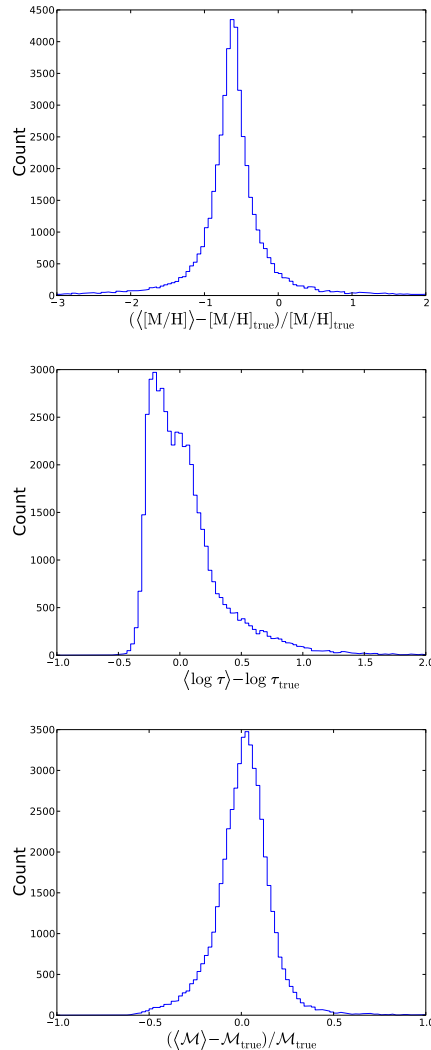


Figure 9. Distributions of residuals (as a fraction of true values in the cases of metallicity and mass) in $[M/H]$, $\log \tau$ and \mathcal{M} , for the correct prior.

duced by clipping the sample at some parallax or parallax error can be avoided.

In Section 3 we used rather a basic characterization of the metallicity distribution of the thin disc. The Geneva-Copenhagen survey (hereafter GCS) is dominated by the thin disc, so it is worthwhile to use the best available model of the thin disc’s metallicity distribution. The analysis of the GCS by Aumer & Binney (2009) found the underlying metallicity distribution to be well fitted by a pdf of the form

$$p_1([\text{Fe}/\text{H}]) = G([\text{Fe}/\text{H}] + 0.12, 0.17), \quad (26)$$

and we used this to represent the metallicity distribution of the thin disc in equation (19), approximating $[M/H] \approx [\text{Fe}/\text{H}]$.

In order to be able to use the Padova isochrones for our analysis of the GCS data, we required magnitudes in the Johnson system for the stars. Since Tycho magnitudes are available for the vast majority of the sample (Perryman 1997), we used the transformation relations of Bessell (2000) to convert these to Johnson magnitudes, assuming a conservative spread of 0.02 mag about the transformation lines.

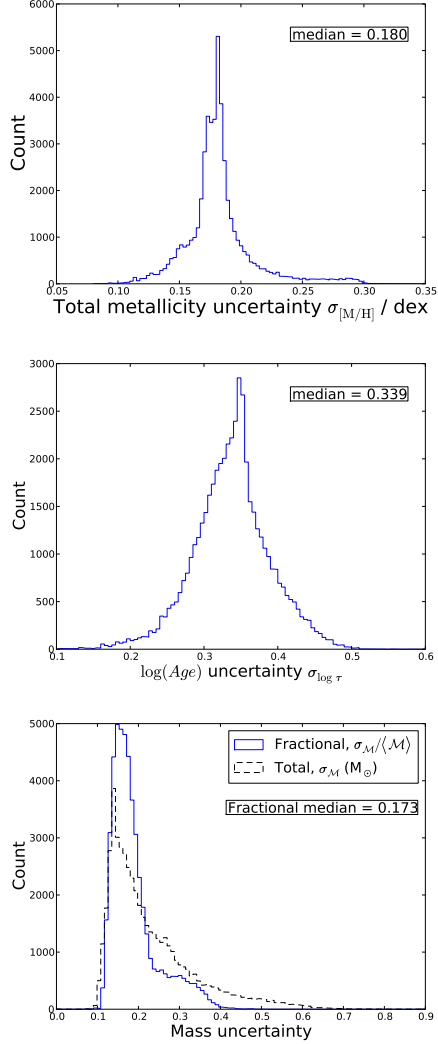


Figure 10. Distributions of uncertainties in $[M/H]$, $\log \tau$ and \mathcal{M} for the correct prior. Uncertainties in metallicity and \log age are absolute; for mass both an absolute error (measured in solar masses) and a fractional error distribution are displayed.

We then generated a pseudodata set to mimic the GCS. For this set, we performed the same procedure as in Section 3, taking

$$\mathbf{y} = (\log T_{\text{eff}}, V, B - V, [M/H]_{\text{obs}}), \quad (27)$$

with the selection function defined by the intersection of the following conditions:

$$P(S|\bar{\mathbf{y}}, \mathbf{x}, \sigma_y) = \begin{cases} 1 & \text{if } 0.28 \leq V - J < 1.72, \\ 0 & \text{otherwise;} \end{cases} \quad (28)$$

$$P(S|\bar{\mathbf{y}}, \mathbf{x}, \sigma_y) = \begin{cases} 1 & \text{if } \log g \geq 3, \\ 0 & \text{otherwise;} \end{cases} \quad (29)$$

$$P(S|\bar{\mathbf{y}}, \mathbf{x}, \sigma_y) = \begin{cases} \frac{\log \overline{T_{\text{eff}}} - 3.6}{0.24} & \text{if } 3.6 \leq \log \overline{T_{\text{eff}}} < 3.84, \\ 0 & \text{otherwise;} \end{cases} \quad (30)$$

$$P(S|\bar{\mathbf{y}}, \mathbf{x}, \sigma_y) = G(\bar{V}^2 - 50, 13). \quad (31)$$

Condition (28) is appropriate because the GCS was designed to limit the survey to F and G stars; the colour cut we have imposed is conservative, permitting stellar types in the range A5–K0 (Binney & Merrifield 1998). Our $\log g$ cut crudely reflects the se-

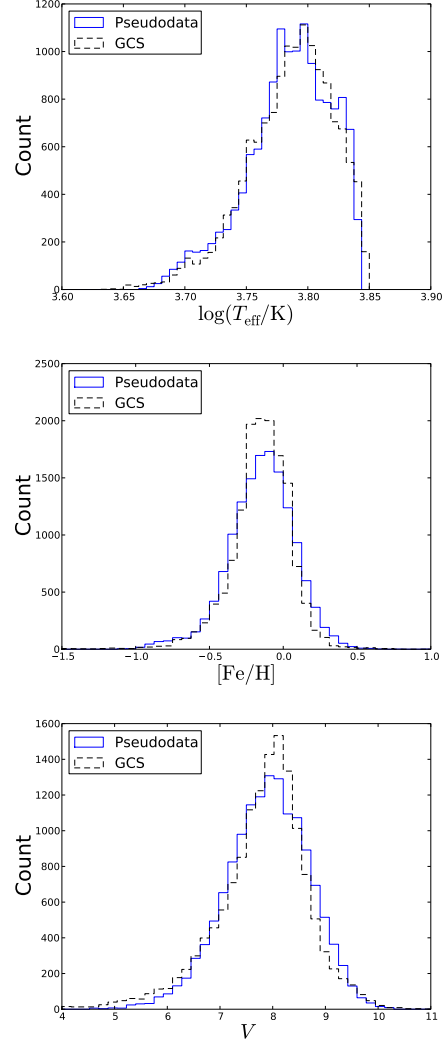


Figure 11. Distribution in effective temperature, metallicity and V -magnitude for our GCS pseudodata (full lines) and star in the real GCS catalogue (dashed lines).

lection against giants that was made on the basis of Strömgren photometry; the other factors are simply based on visual inspection to provide a reasonable mimic of the actual distributions of the data in observable space. We also imposed a Gaussian error distribution on the ‘measured’ parallax with dispersion

$$\sigma_{\varpi} = \begin{cases} 0.3 \text{ mas} & \text{if } \bar{V} < 5, \\ (0.3 + 0.06(\bar{V} - 5)^2) \text{ mas} & \text{otherwise,} \end{cases} \quad (32)$$

based on an approximate fit to the variation of Hipparcos’ parallax error with apparent V -magnitude. The resultant match is displayed in Fig. 11.

For the analysis of the GCS data it was decided to take

$$\phi(\mathbf{x}) = \begin{cases} 1 & \text{if } 0.28 \leq V - J < 1.72, \\ 0 & \text{otherwise,} \end{cases} \quad (33)$$

and the prior $p(\mathbf{x})$ from equation (18) ff. Including a $\log g$ dependency within $\phi(\mathbf{x})$ would have been possible, but it was felt to be too haphazard to simply cut away all stars with e.g. $\log g < 3$, since the GCS selection was made on the basis of Strömgren colours and not on direct measurements of surface gravity. Consequently we

analysed both the pseudodata and the real GCS data using a selection function as in equation (33). The fitting was performed in the variables $(\log T_{\text{eff}}, V, B - V)$, since we were not confident in the precision of matching $[M/H]$ to $[Fe/H]$.

In Fig. 12 we display the results of analysis of both the pseudo-data and the true GCS sample; both samples contained 14 233 stars. It can be seen that the match is very good. In the first and fourth panels we display the mean and standard deviation of each distribution. To find these values for our analysis of the true data we have clipped 62 outliers with x -axis values below -6 . The total uncertainty in the first panel, $\sigma_{\varpi}^{\text{total}}$, is found from adding our output uncertainty and the Hipparcos error in quadrature. The uncertainties in the third and fourth panels are those purely due to our method; the fourth panel displays the normalized residuals for the pseudo-data analysis when one does not include any observational error in the ‘observed’ parallax measurements. It is clear from Fig. 12 that our method works convincingly on real data. Fig. 13 shows the output from applying a maximum likelihood analysis to the same data, and it can be seen that the results are comparable to those from section 3: the mean of the normalized residuals distribution is significantly biased, falling at a value of 0.50.

4.1 Binary stars

The method developed here is properly applicable only to single stars; however binaries with a mass ratio reasonably far from unity will not present a significant problem since the observations can be expected to capture the properties only of the more massive star. It is instructive to consider the worst case – that of two equally massive stars – in which the absolute magnitude will be 0.75 mag brighter than for one of the stars. If all other observables are as they would be for one of the stars, this can be expected to result in an underestimate of the distance by around 29 per cent. Fig. 3 demonstrates that this is within, or on the order of, the output uncertainties for virtually all stars due to the underlying physics, and thus does not dramatically compromise our results.

The GCS catalogue makes an empirical test of this theory possible. Fig. 14 shows the histogram of normalized parallax residuals for our analysis of the GCS data, divided into those that have been flagged in the GCS catalogue as a probable binary, and those without this flag. Each group is labelled with its mean and dispersion after cutting outliers at $x < -6$. The photometric parallaxes of the binaries are larger than their measured parallaxes by 0.17σ in the mean, while the parallaxes of the single stars are 0.11σ smaller in mean than their measured parallaxes. Since $\sigma/\varpi \sim 0.36$ (Fig. 12), this level of bias corresponds to ~ 6 per cent for each star, which lies well within the predicted worst-case level. Moreover, since the probability that a given system will be flagged as a binary is an increasing function of received flux, and therefore of *true* parallax, flagged stars may be expected to have Hipparcos parallaxes that are on average slightly smaller than their true parallaxes. This can be seen by considering an imaginary sample of stars with a single measured Hipparcos parallax; these stars will have been scattered by observational errors from true parallaxes both above and below the measured value. If one then selects, independently, stars with a preferentially larger true parallax, one will obtain a sample which is fundamentally biased to true parallaxes greater than the Hipparcos measurements. Expanding this reasoning to the entire Hipparcos sample, it must hold for every measured parallax, and thus one expects the subsample flagged as binaries to be biased in exactly this manner. Consequently the amount by which our photometric parallaxes exceed the true parallaxes is likely to be smaller than the

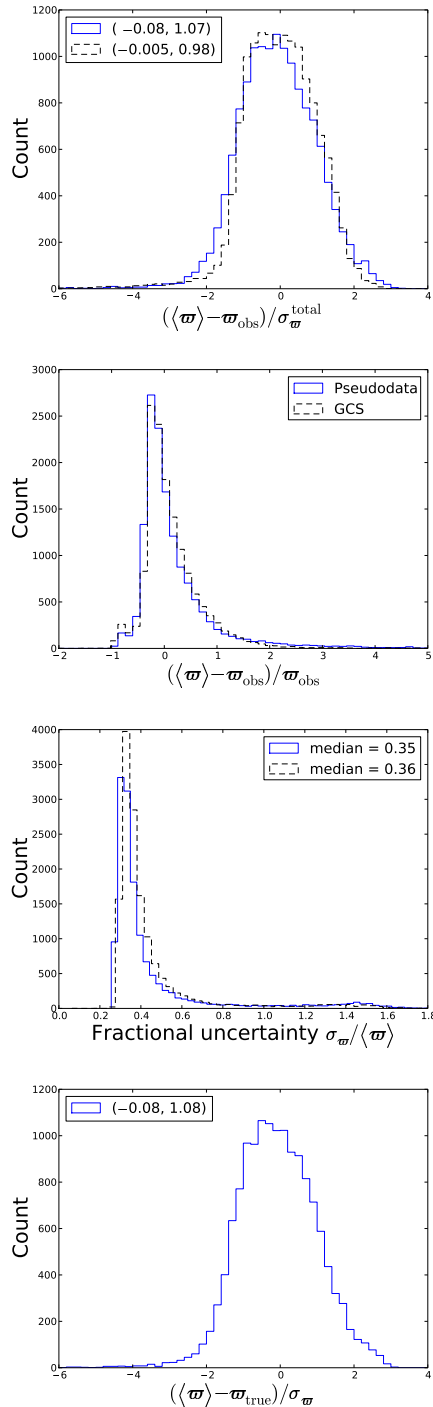


Figure 12. Photometric parallaxes from GCS pseudodata (blue lines, full) and from the real GCS sample (black lines, dashed). Top panel: the normalized distribution of parallax residuals; ϖ_{obs} is obtained by adding the errors returned by the method and the Hipparcos errors in quadrature. Each line is labelled by (mean, dispersion). Second panel: distribution of residuals as a fraction of true parallax. Third panel: distribution of fractional photometric (output) uncertainties. Bottom panel: equivalent to the top panel but showing true normalized residuals for the pseudodata, removing the ‘observational’ error.

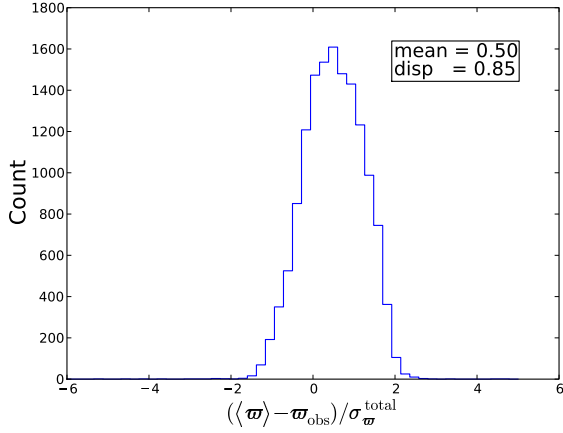


Figure 13. Normalized parallax residuals for the real GCS sample for a maximum likelihood analysis.

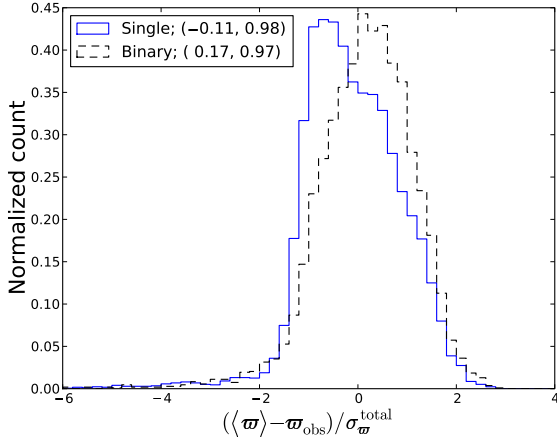


Figure 14. Histogram of the normalized residuals in parallax space for stars thought to be single (blue line, full) and those flagged as binaries (black line, dashed). For each distribution, the mean and dispersion are displayed in the legend.

amount by which they exceed the Hipparcos parallaxes. In fact this effect may also account for the discrepancy between the photometric and Hipparcos parallaxes of ‘single’ stars: many of these objects will be binary stars that are too distant to be resolved, and it is likely that in more than half of these cases accidental errors have boosted rather than diminished the Hipparcos parallax.

4.2 Parallax vs distance

It is of interest to inspect the results of our analysis of the GCS in distance as well as in parallax. Fig. 15 shows a plot of the distribution of output fractional uncertainties in distance against fractional uncertainties in parallax. It follows a rather peculiar ‘high-heeled shoe’ shape. We can explain the general form of this distribution by considering two highly simplified forms for a star’s distance pdf. Inspection of the pdf for stars in the ‘heel’ of the shoe ($\sigma_{\varpi}/\langle\varpi\rangle \sim 0.3$) shows the typical pdf to be reasonably approximated by a single power-law with a low- s cutoff, i.e.

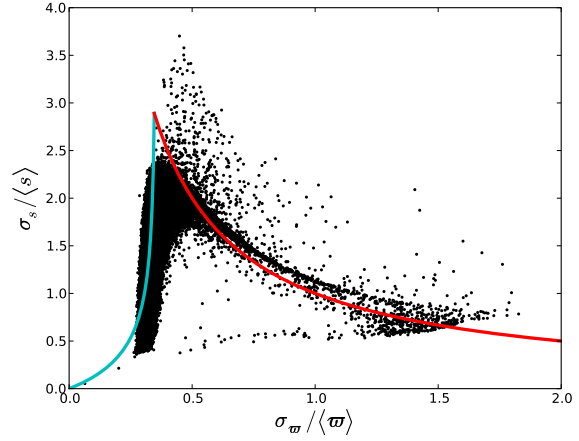


Figure 15. The distribution of stars in fractional error space, from analysis of the GCS data. Fit curves are described in Section 4.

$$p(s) \propto \begin{cases} 0 & \text{for } s < a, \\ s^{-\alpha} & \text{otherwise.} \end{cases} \quad (34)$$

If we calculate the moments of this highly simplified pdf we find that, letting $X \equiv \sigma_{\varpi}/\langle\varpi\rangle$ and $Y \equiv \sigma_s/\langle s\rangle$, we should expect the relation

$$\sqrt{1 + X^{-2}} + \sqrt{1 + Y^{-2}} = 2, \quad (35)$$

which is overplotted on Fig. 15 and can indeed be seen to fit the heel of the shoe.

Regarding stars on the ‘sole’ of the shoe, inspection of their pdfs in distance reveals them to be largely bimodal. As a very crude approximation of this we can take

$$p(s) = \beta \delta(s - s_1) + (1 - \beta) \delta(s - \eta s_1), \quad (36)$$

where $\delta(x)$ represents the Dirac delta function. The resultant moments are not trivial, but if we consider only the case in which $\eta \gg 1$, we obtain

$$(X, Y) \approx \left(\sqrt{\frac{1 - \beta}{\beta}}, \sqrt{\frac{\beta}{1 - \beta}} \right) \Rightarrow Y \approx \frac{1}{X}, \quad (37)$$

which is also overplotted on Fig. 15 and provides a good fit to the sole of the shoe, despite the crudeness of the approximation.

The fact that this extremely simplistic widely-spaced bimodal distribution provides such a good fit to Fig. 15 conceals an important fact. It is related to the lack of $\log g$ information in the GCS data in the form that we have used them: the distance-fitting algorithm has essentially no way of distinguishing between dwarfs and giants for many of the stars, resulting in two widely-spaced peaks in the distance pdf. The large uncertainties on the distance reflect this lack of discrimination, providing an even more cogent argument than that of Fig. 6 for the necessity of tight observational constraints on $\log g$ if accurate spectrophotometric distances are to be obtained. In this case it is clear that the best choice for an indication of each star’s position is actually given by its measured parallax and the uncertainty thereon, as opposed to the direct distance determination provided by the method.

Since the GCS stars virtually all have Strömgren photometry, it is of interest to study the results from running our method when these data are included. To do this we need a set of stellar models that provide Strömgren magnitudes. The BaSTI isochrones (Cassisi et al. 2006) provide such models. We used the $[\text{Fe}/\text{H}]$ val-

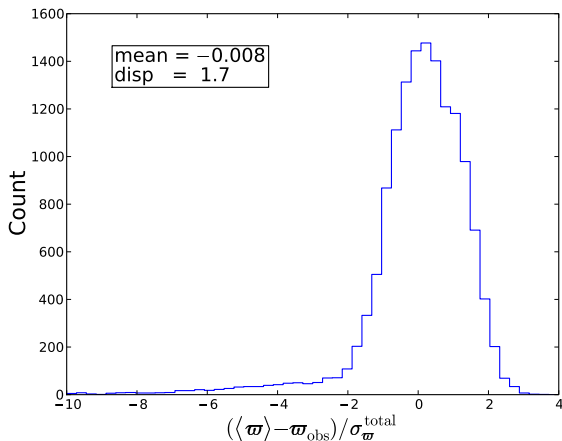


Figure 16. The distribution of normalized residuals from an analysis of the GCS data using the BaSTI stellar models.

ues in the set

$$[\text{Fe}/\text{H}] \in \{-2.27, -1.79, -1.49, -1.27, -0.96, -0.66, -0.35, -0.25, 0.06, 0.26, 0.40\}.$$

Unfortunately, it proved impossible to obtain a convincing match between these models and the data: for many GCS stars ($\sim 11\,000$ of the 14 233) no BaSTI model lay within $\sim 2\sigma$ of its measured properties – the errors on the GCS data are ~ 0.01 in $\log T_{\text{eff}}$ (Nordström et al. 2004) and ~ 0.003 in $b - y$ (Olsen 1983, 1993, 1994a,b). It is also clear from an inspection of the data that a simple systematic shift in effective temperature cannot solve this problem. In an attempt to work around this difficulty, we dropped $b - y$ from \mathbf{y} , making the observational constraints

$$\mathbf{y} = (\log T_{\text{eff}}, V, m_1, c_1, [\text{Fe}/\text{H}]_{\text{obs}}), \quad (38)$$

and we enlarged the errors in photometry to ten times their quoted medians; hence

$$\sigma_{\mathbf{y}} = (0.01, 0.05, 0.04, 0.06, 0.1). \quad (39)$$

We maintained the same prior as for our previous analysis, and took a flat $\phi(\mathbf{x})$. The resultant histogram of normalized parallax residuals is displayed in Fig. 16, along with the mean and dispersion of the distribution. It can be seen that although the distribution is, as ever, unbiased, the errors in this case have been noticeably underquoted, resulting in a dispersion of 1.7 in the distribution of normalized residuals. This is hardly surprising given the questionable nature of the fit between the models and the observations. Fig. 17 shows that the distribution of the stars in error space is similar to that of Fig. 15; however, since the top of the shoe occurs at ~ 1.4 rather than ~ 2.5 , the distance errors are now smaller, reflecting the fact that the Strömgren colours give a significantly better handle on the dwarf/giant dichotomy than standard Johnson colours.

5 RELATION TO PREVIOUS WORK

It is worth briefly considering the difference between the technique presented here and that employed on the second RAVE data release by Breddels et al. (2010). Breddels et al. estimate the distance to each star by finding the model star that gives the smallest chi-squared value when its observables are compared with the observations. Then 5 000 ‘observed’ realizations of the model star are

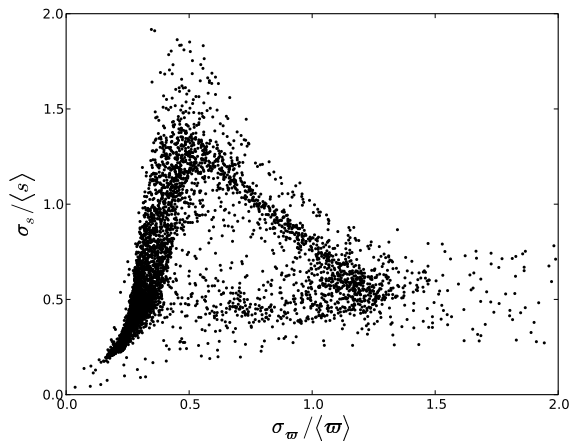


Figure 17. The distribution of stars in fractional error space, from analysis of the GCS data using the BaSTI stellar models and Strömgren photometry.

produced by scattering the observables of the best-fitting star with errors drawn from a Gaussian in \mathbf{y} -space, of width determined by the stated observational errors. Finally the model that best fits each of these 5 000 pseudo-stars is found, and the mean and variance of the absolute magnitudes of the 5 001 best-fitting models is calculated.

This technique can be viewed as a form of maximum-likelihood estimation: it essentially involves considering only the likelihood term $p(\bar{\mathbf{y}}|\mathbf{x}, \sigma_{\mathbf{y}})$ from our equation (7). The main shortcoming of the procedure is that it fails to take advantage of the fact that some types of star are extremely rare, so it is much more likely that a particular datum reflects bad luck with the observations than detection of a very rare type of star, such as a young, very metal-poor star, whose true observable coincides with the datum. Incorporation of the selection function and the prior allows the computer to choose the model star that is the sanest choice.

There is an additional problem with the procedure used by Breddels et al.: in the event that the data lie say 2σ from the true values of the star’s observables, the method involves fitting model stars to data points that lie 3 or even 4σ from the true value. Compounding errors in this way is not sensible.

Zwitter et al. (2010) have recently made significant improvements on the work of Breddels et al., introducing a mass prior and a more sophisticated treatment of the RAVE errors, as well as exploring the effects of different sets of stellar models.

Jørgensen & Lindegren (2005), building on the work of Pont & Eyer (2004) (see appendix A), developed a Bayesian method for the estimation of stellar ages (which extends naturally to other parameters), involving a very simple prior and marginalization over all parameters except the one of interest. The concept of regarding distance as a stellar parameter as we do in this paper was not explored.

Jørgensen & Lindegren use the mode to characterize each distribution, a decision with which we disagree for the reasons given in Section 2. Confidence intervals, which they used to characterize errors, are good measures but in general comparatively difficult to calculate, and more importantly require interpolation in the isochrones, which we have endeavoured to avoid.

The prior used in the analysis of Jørgensen & Lindegren is extremely simple: it is flat in both metallicity and age, although in initial mass it is a single power law, representative of a simple IMF.

While the rationale for this choice is well-established, we feel that it does not take advantage of the large body of prior knowledge that we have regarding the samples with which we are dealing: the Galaxy is certainly not, for example, uniformly distributed in age. It seems logical to exploit all the information that is available, and that includes our significant previous knowledge of the distributions of each stellar parameter throughout the Galaxy.

An important point relevant both to the work of Jørgensen & Lindegren and that of Breddels et al. regards speed: Jørgensen & Lindegren’s technique of analysing the marginalized pdf for the stellar age (or mass in Nordström et al. 2004) does not permit the versatility of calculation that our method provides: by considering the distance as an intrinsic parameter of each star, on the same footing as its metallicity, age and mass, we are able to provide a consistent and simultaneous (and therefore rapid) determination of the values of all four parameters for each star, without requiring successive marginalizations that would significantly slow the analysis. Likewise the technique of Breddels et al. requires the solution of 5 001 optimization problems for every star, as opposed to a single-pass integration. Our technique therefore represents a significant improvement in efficiency, which is particularly relevant in the analysis of the large surveys that are both under way and planned.

6 CONCLUSIONS

We have presented a Bayesian technique for determining stellar parameters from photometric and spectroscopic data. It has been demonstrated that the technique outperforms maximum-likelihood techniques, and the mathematical and physical basis of the system ensures that all available information can be exploited in the calculation. The resultant uncertainties, assuming a reasonable prior is chosen, are therefore a consequence purely of the underlying physics, and by virtue of this the technique is optimal – given a set of data and some level of understanding of the underlying physics, one cannot do better. Since the uncertainties derived from our technique simply reflect the physics, so long as one employs a reasonable prior, the technique will provide the most accurate possible estimates of the true uncertainties – smaller estimated uncertainties could only come from an overly restrictive prior, undersampling the pdf in some manner or defining the uncertainties in a different manner, as for example in Jørgensen & Lindegren (2005).

The problem of fitting stellar models to observations is an ideal setting for the application of Bayesian probability theory. We have a wealth of advance knowledge of the underlying physics with which to construct a prior, and the complex relationship between input parameters and observables for stellar models renders a simple maximum-likelihood approach suboptimal for providing reliable parameter determinations. There *are* favoured regions of observable space; our approach exploits this by virtue of the input prior. The Bayesian method also enables a valuable synthesis of different areas of astrophysical research: large-scale analysis and mapping of stellar populations in the Galaxy feeds us information for the prior, whilst the specifications of observations give us the form of the likelihood and selection functions.

As with all photometric techniques, obscuration, which we have neglected, is an important issue. It would be simple to include reddening and extinction models, but inevitably the results would then be vulnerable to weaknesses in the adopted models. When a large body of trigonometric parallaxes for relatively distant stars is at hand, it will be possible to adjust such models by making pho-

tometric distances compatible with trigonometric parallaxes. Such work will be a key project to be undertaken with the Gaia Catalogue.

A simplification we have made is to consider all metallicity information to be encoded in the value of $[M/H]$ for each star. The chemistry of stars is in reality more complex and both helium abundance and alpha enhancement play significant roles in stellar evolution. We have not explicitly addressed this issue because to do so we would require both further sets of isochrones and additional spectroscopic observables. However, such refinements will be possible within a decade; most importantly, their incorporation would represent no fundamental change to the method presented here.

While our method is strictly only applicable to single stars, dividing the GCS sample into probable binaries and single stars reveals that the parallaxes of binaries are under-estimated by at most $\sim 0.2\sigma$ in the mean, and probably by only half this figure (Section 4.1). The effect of binarity on the estimation of other stellar parameters is more subtle, however Jørgensen & Lindegren (2005) provide a demonstration that its effect on Bayesian age determination is quite limited. The effect of binaries could be incorporated into our formalism by including a probability of binarity in the prior, along with its associated effect on the various observables; this is the approach taken in the work of Pont & Eyer (2004). Taking full account of such contamination would require observational simulations to find the effect of different mass-ratio binaries on each observable.

In this work we have introduced the selection function $P(S|\bar{y}, \mathbf{x}, \sigma_y)$ as an explicit term in our calculations. Its inclusion provides an intuitive and logically consistent means of taking account of all selection effects introduced by instrumental apparatus, observing strategies and later choices (such as cuts on errors to ‘clean’ a sample). The presence of this factor in our calculations in the form of $\phi(\mathbf{x})$ is key, as it truly brings the model to the data rather than vice versa, and thus permits a theoretically much more satisfactory basis for all our calculations.

The distribution defined by the product of the selection function and the prior has another use. This distribution can be used as in equation (17) to generate a sample of pseudodata, which can then be scattered by Gaussian ‘observational errors’. The distributions of the various observables of this pseudodata can then be compared with those of the true data set that one wishes to mimic, in order to assess the accuracy of the different factors one has included. Thus, if one is confident of the selection function (as will often be the case), one can adapt the prior until a good fit is found between the pseudodata and the real data. Once this has been achieved, this optimized prior can then be used in the analysis of the true data with a high degree of confidence.

In this work the form of the prior has been kept intentionally simple: we have dealt with a case in which the Galaxy is described by three stellar populations. Depending on the nature of the sample being analysed, the prior could take a large range of forms. An interesting case that we have not considered is when the data include kinematic quantities. Then the prior would include a full phase-space distribution function for each stellar population, and this enrichment of the prior information that is brought to bear on the data would further reduce the uncertainties in estimated distances, metallicities, etc. Indeed the power of the Bayesian method described in this paper lies in its generality; although it was applied only to spectrophotometric data in Sections 3 and 4, nothing restricts the inclusion of other observables.

Of course the correct form for the prior is unlikely to be known absolutely. One may however be able to specify it with a reason-

able degree of certainty – one might, for example, be able to give the prior in a parametric form with a certain pdf over the parameters that specify it (such as disc scale lengths). The integration described in Section 2 can then also be performed over these parameters, providing slightly less assumption-dependent values for the method's outputs.

We have not explored the question of the joint probability distributions of different parameters conditional upon the data for each star. Using the same technique as we describe but marginalizing only over selected dimensions of \mathbf{x} , it would be possible to examine such distributions and analyse covariances between different parameters for selected stars. This extension would be simple and one can envisage cases in which it could prove fruitful.

Another consideration regarding the pdf for each star is that of bimodality. We have characterized each star's pdf in distance by its mean and dispersion; however an extension of this approach would be to search through each star's pdf in distance to identify any instances of multimodality. Some stars essentially present two distinct solutions for the given observables: one being a dwarf lying comparatively nearby, the other a more distant giant (as in the cases explored for the GCS in Section 4). It could be fruitful to identify such degeneracies explicitly, and provide a mean and dispersion for each peak in the pdf. Starting from the algorithm described in this paper, one could identify any points in the assigned grid whose probabilities (by equation 7) lie above some chosen threshold value, and then seek to identify sizeable islands in this subset of the space by a friends-of-friends type algorithm (Huchra & Geller 1982). This would provide a method of partitioning the pdf into discrete distributions, each of which could then be assigned an average value and associated spread. Thus significant degeneracies in the pdf resulting from certain values of the observables could be identified and handled suitably. We hope to explore this avenue in a future paper.

We have shown that by using all of the available information one can constrain the metallicities of stars to greater accuracy than the observations themselves. It is reasonable to expect that this same effect can be achieved for other observable quantities such as the surface gravity, for which the nominal observational errors are often sizeable. In this manner one can use the small errors on certain observables (such as apparent magnitudes) to shrink conservative errors on less well-constrained values. So long as one has confidence in the stellar models used, this promises to be a powerful technique for survey analysis. It should be noted that this technique can only realistically be applied once – 'looping', by rerunning the analysis using the new values and errors, is prohibited – since its effectiveness comes from the application of independent prior knowledge to data with mildly overquoted errors. The mathematical formalism does not permit the subsequent application of a prior that is not independent of the data.

One more point deserves mention. If one knows the distances to the stars in some specific sample (of a generic type that can be described by model isochrones), then one can in theory explore different forms for the prior in order to optimize one's estimation of their distances. This could then be fed back in to the algorithm in order to provide a more accurate estimation of distances to other stars.

We are currently using this method to obtain distances to in excess of 250 000 RAVE stars and hope shortly to report the results of this work.

ACKNOWLEDGMENTS

Thanks are due to John Magorrian and the other members of the Oxford dynamics group for many helpful comments on this work. BB also thanks Michael Aumer for his initial help with isochrone handling, and acknowledges the support of PPARC/STFC.

REFERENCES

- Aumer M., Binney J. J., 2009, *MNRAS*, 397, 1286
 Bertelli G., Girardi L., Marigo P., Nasi E., 2008, *A&A*, 484, 815
 Bessell M. S., 2000, *PASP*, 112, 961
 Binney J., Merrifield M., 1998, *Galactic astronomy*. Princeton University Press, Princeton, NJ
 Breddels M. A., Smith M. C., Helmi A., et al. 2010, *A&A*, forthcoming
 Carollo D., Beers T. C., Chiba M., Norris J. E., Freeman K. C., Lee Y. S., Ivezić Z., Rockosi C. M., Yanny B., 2009, *ArXiv e-prints*
 Cassisi S., Pietrinferni A., Salaris M., Castelli F., Cordier D., Castellani M., 2006, *Memorie della Societa Astronomica Italiana*, 77, 71
 Eyre A., 2009, *MNRAS*, submitted
 Eyre A., Binney J., 2009, *MNRAS*, 399, L160
 Gautschi A., Saio H., 1996, *ARA&A*, 34, 551
 Gillessen S., Eisenhauer F., Trippe S., Alexander T., Genzel R., Martins F., Ott T., 2009, *ApJ*, 692, 1075
 Haywood M., 2001, *MNRAS*, 325, 1365
 Holmberg J., Nordström B., Andersen J., 2009, *A&A*, 501, 941
 Huchra J. P., Geller M. J., 1982, *ApJ*, 257, 423
 Jaynes E., 2003, *Probability Theory: The Logic of Science*. Cambridge University Press, Cambridge
 Jin S., Lynden-Bell D., 2008, *MNRAS*, 383, 1686
 Jørgensen B. R., Lindegren L., 2005, *A&A*, 436, 127
 Jurić M., Ivezić Ž., Brooks A., et al. 2008, *ApJ*, 673, 864
 Kroupa P., Tout C. A., Gilmore G., 1993, *MNRAS*, 262, 545
 Nordström B., Mayor M., Andersen J., Holmberg J., Pont F., Jørgensen B. R., Olsen E. H., Udry S., Mowlavi N., 2004, *A&A*, 418, 989
 Olsen E. H., 1983, *A&AS*, 54, 55
 Olsen E. H., 1993, *A&AS*, 102, 89
 Olsen E. H., 1994a, *A&AS*, 104, 429
 Olsen E. H., 1994b, *A&AS*, 106, 257
 Perryman M., 1997, *The Hipparcos and Tycho Catalogues*. Noordwijk: ESA Publications
 Perryman M. A. C., 2005, in P. K. Seidelmann & A. K. B. Monet ed., *Astrometry in the Age of the Next Generation of Large Telescopes Vol. 338 of Astronomical Society of the Pacific Conference Series, Overview of the Gaia Mission*. pp 3–
 Pont F., Eyre L., 2004, *MNRAS*, 351, 487
 Reddy B. E., 2009, *ArXiv e-prints*
 Saha P., 2003, *Principles of Data Analysis*. Cappella Archive, Great Malvern, England
 Skrutskie M. F., Cutri R. M., Stiening R., et al. 2006, *AJ*, 131, 1163
 Steinmetz M., 2003, in Munari U., ed., *GAIA Spectroscopy: Science and Technology Vol. 298 of Astronomical Society of the Pacific Conference Series, RAVE: the RADial Velocity Experiment*
 Steinmetz M., Zwitter T., Siebert A., et al. 2006, *AJ*, 132, 1645
 Zwitter T., Matijević G., Breddels M. A., et al. 2010, *ApJS*, p. submitted

Zwitter T., Siebert A., Munari U., et al. 2008, AJ, 136, 421

This paper has been typeset from a $\text{\TeX}/\text{\LaTeX}$ file prepared by the author.

APPENDIX A: JACOBIAN QUESTIONS

There is some confusion in the literature regarding the necessity or otherwise of a Jacobian term in the transition from considering the likelihood term as a function of \mathbf{x} to considering it implicitly as a function of $\mathbf{y}(\mathbf{x})$ (such as when it is converted to the form $G(\bar{\mathbf{y}} - \mathbf{y}(\mathbf{x}), \boldsymbol{\sigma}_y)$). The Borel-Kolmogorov paradox (see, for example, Jaynes 2003) cautions that this step should be taken with care. However, it is a simple matter to demonstrate that the term is unnecessary.

If we consider, for a moment, \mathbf{y} not to be a function of \mathbf{x} but rather to be described by a pdf on \mathbf{x} , we can expand equation (7):

$$p(\mathbf{x}|\bar{\mathbf{y}}, \boldsymbol{\sigma}_y, S) \propto P(S|\bar{\mathbf{y}}, \mathbf{x}, \boldsymbol{\sigma}_y) p(\bar{\mathbf{y}}|\mathbf{x}, \boldsymbol{\sigma}_y) p(\mathbf{x}) \quad (\text{A1})$$

$$= P(S|\bar{\mathbf{y}}, \mathbf{x}, \boldsymbol{\sigma}_y) \left(\int p(\bar{\mathbf{y}}|\mathbf{y}', \mathbf{x}, \boldsymbol{\sigma}_y) p(\mathbf{y}'|\mathbf{x}) d\mathbf{y}' \right) p(\mathbf{x}); \quad (\text{A2})$$

but then we can express the true functional dependence of \mathbf{y}' by

$$p(\mathbf{y}'|\mathbf{x}) = \delta(\mathbf{y}' - \mathbf{y}(\mathbf{x})), \quad (\text{A3})$$

leading directly to

$$p(\mathbf{x}|\bar{\mathbf{y}}, \boldsymbol{\sigma}_y, S) \propto P(S|\bar{\mathbf{y}}, \mathbf{x}, \boldsymbol{\sigma}_y) p(\bar{\mathbf{y}}|\mathbf{y}(\mathbf{x}), \boldsymbol{\sigma}_y) p(\mathbf{x}), \quad (\text{A4})$$

which contains no Jacobian.